Russian Chemical Reviews **75** (4) 303 – 315 (2006) © 2006 Russian Academy of Sciences and Turpion Ltd

DOI 10.1070/RC2006v075n04ABEH002548

Spatially resolved atomic absorption spectrometry

A Kh Gilmutdinov, A V Voloshin, K Yu Nagulin

Contents

I.	Introduction	303
II.	Spatial distribution of transmitted radiation intensity	304
III.	Dynamics of spatial temperature distributions in atomisers	306
IV.	Three-dimensional structures of absorbing layers	306
V.	Influence of spatial inhomogeneities of absorbing layers on absorption	310
VI.	Spatially resolved atomic absorption analysis	311
VII.	Conclusion	314

Abstract. The review provides an overview of the main steps of development of spatially resolved atomic absorption spectrometry. The results of research on the dynamics of spatial distributions of atoms, molecules, condensed nanoparticles, temperature fields in atomisers and the transmitted radiation intensity are generalised. The influence of spatial inhomogeneities on the formation of absorption signals is considered. The advantages of spatially resolved atomic absorption spectrometry are illustrated with examples. The bibliography includes 82 references.

I. Introduction

Due to high sensitivity and selectivity, atomic absorption spectrometry (AAS) has found wide application in physics (in measurements of oscillator strengths, diffusion coefficients, gas temperatures, *etc.*), astrophysics (in studies of the chemical composition of stars) and physical chemistry (for the determination of the saturated vapour pressure, heats of vaporisation, rate constants, *etc.*). However, this method is most widely used in analytical chemistry. This technique provides the basis of atomic absorption analysis as a method of quantitative chemical analysis based on atomic absorption spectra. Nowadays, analytical atomic absorption spectrometry is one of the most commonly used methods for elemental analysis.[1] Initially, flame atomic absorption spectrometry has been developed.[2] However, AAS with electrothermal atomisation has received most attention in more recent years.[3] The use of semiclosed graphite tube atomisers made it possible to reduce the method detection limit by a factor of $\sim 10^3$. As a result, it becomes possible to perform microanalysis and direct analysis of solid substances and suspensions. Presently, more than 60 chemical elements can be determined by AAS at ppb (or lower) levels in virtually all substances and materials.[4]

A Kh Gilmutdinov, A V Voloshin, K Yu Nagulin Department of Physics, Kazan State University, ul. Kremlevskaya 18, 420008 Kazan, Russian Federation. Fax (7-843) 231 52 20, tel. (7-843) 231 53 64, e-mail: Albert.Gilmutdinov@ksu.ru (A Kh Gilmutdinov), Alexandr.Voloshin@ksu.ru (A V Voloshin), Konstantin.Nagulin@ksu.ru (K Yu Nagulin)

Received 3 October 2005
Uspekhi Khimii **75** (4) 339 – 353 (2006); translated by T N Safonova

Atomic absorption spectrometry is based on interaction of transmitted radiation (generally, at the resonance wavelength λ) with a cloud of free analyte atoms produced in an atomiser. The larger the amount of absorbing atoms in the gas phase in an atomiser, the stronger the absorption of transmitted radiation. Two aspects of this interaction can be distinguished. First, the absorption depends on the overlap of the spectral profile of the analytical line of the radiation source $J(\lambda)$ with the absorption line profile of the analyte atoms $k(\lambda,T)$ (Fig. 1 *a*). The mechanism of this interaction, which can be referred to as the spectral interaction, has been studied and described in detail.[5, 6]

The absorbance (A), which is determined as the logarithm of the ratio of the luminous flux (Φ_0) incident on the absorbing layer to the flux passed through the atomiser (Φ_t), serves as the quantitative measure of absorption. The absorbance in AAS plays the same role as the analytical line intensity in atomic emission spectrometry. If the spectral linewidth of transmitted radiation is substantially smaller than the absorption linewidth, the absorbance of a spatially homogeneous absorbing layer is directly proportional to the number of absorbing atoms (N) as follows from the Bouguer – Lambert – Beer law

$$A = \log\frac{\Phi_0}{\Phi_t} = C(\lambda,T)\,N, \qquad (1)$$

where the coefficient $C(\lambda,T)$ depends on the atomiser temperature and accounts for the spectral features of the analytical line. Taking

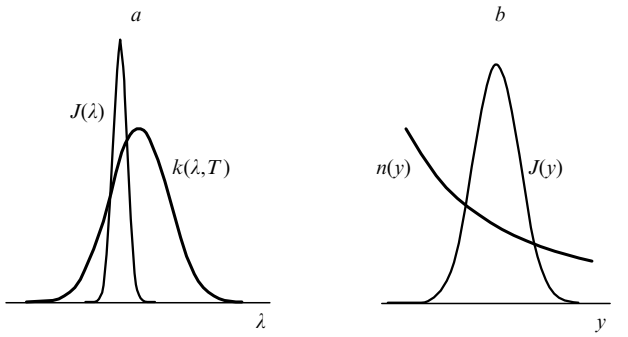


Figure 1. Scheme illustrating spectral (*a*) and spatial (*b*) interactions of the transmitted radiation beam with an absorbing layer.
T is the atomiser temperature.

into account broadening and shifts of the spectral lines and the hyperfine structure of the spectral transition, linear dependence (1) is violated: each factor leads to a decrease in the slope of the plot and its curving in the high-absorption region.[4]

Another aspect of interaction is associated with spatial inhomogeneity of the absorbing layer and the transmitted radiation intensity. The transmitted beam characterised by the intensity distribution $J(x,y,z)$ is absorbed by atoms and molecules non-uniformly distributed in an atomiser $n(x,y,z)$. This aspect can be referred to as the spatial interaction (Fig. 1 *b*).

Evidently, the atomic absorption depends not only on the spectral characteristics of the analytical line but also on the characteristic features of the spatial distribution of the analyte atoms and the probe beam. In addition, it should be taken into account that absorption of transmitted radiation occurs in the volume of an atomiser characterised by spatially inhomogeneous temperature fields. However, in spite of this fact, AAS has been developed over many years with consideration only for spectral interaction,† because it has been implicitly assumed that the absorbing layer in the cross-section of an atomiser is spatially homogeneous. In this case, $n(y) = \text{const}$ (see Fig. 1 *b*), and the detected absorption is independent of the transmitted radiation intensity distribution. This assumption was not in doubt because atomisation temperatures are thousands of degrees centigrade and it seemed reasonable that all spatial inhomogeneities would be smoothed in the transmitted beam with a height of only 2 – 5 mm due to fast gas-phase diffusion. However, more recently it has been demonstrated that all key parameters of AAS, *viz*., the temperature of the absorption zone and the distributions of atoms, molecules and condensed species, are characterised by substantial non-uniformity. In this connection, the need arose to take into account the spatial factor.

The present review briefly summarises the results and the state of the art in the field of spatially resolved AAS, which equally takes into account both the spectral and spatial aspects of interactions between the resonance radiation and absorbing atoms. Initially, the spatial distributions of the transmitted radiation intensity, absorbing atoms, molecules and condensed species and the temperature fields in the volume of an atomiser are considered. Then analysis of the influence of the non-uniformity of the distributions of these parameters on the atomic absorption is presented and the ways of eliminating this influence are described. Finally, examples of the analytical use of spatially resolved AAS are given and this method is compared with conventional AAS (where spatial inhomogeneities are ignored).

II. Spatial distribution of transmitted radiation intensity

1. Hollow cathode lamps

Hollow cathode lamps are the most common transmitted radiation source for AAS. Narrow (with a width of about 1 pm) spectral lines $J(\lambda)$ of analyte atoms are generated in the glow discharge plasma in a hollow cylindrical cathode. The cathode material includes the analyte element, the line spectrum of which is necessary to record. This chemical element is introduced into the plasma by vaporisation of the cathode by fill gas ions (generally, neon or argon) at a pressure of a few Torr. Results of studies of physical processes occurring in the glow discharge plasma and the spectral characteristics of the generated radiation are summarised in reviews.[5–9] The spatial characteristics of the radiation beam from hollow cathode lamps at resonance and non-resonance lines of different elements and the atomic and ionic lines of a fill gas were studied in-depth.[10–12] The character of the spatial distribution of the spectral intensity in hollow cathode lamps was demonstrated to depend primarily on the cathode radius. A typical distribution of the spectral intensity in the cross-section of a hollow cathode lamp is illustrated in Fig. 2 *a*. The radiation was detected at the resonance wavelength of lead (283.3 nm). The distribution is dome-shaped, has an intensity maximum at the cathode axis and decreases monotonically to zero at the ends of the cathode. These distributions are characteristic of not only the metal lines but also the fill gas lines and are well described by parabolic functions. This is indicative of charge localisation in the cathode hollow and direct electron impact excitation of metal and

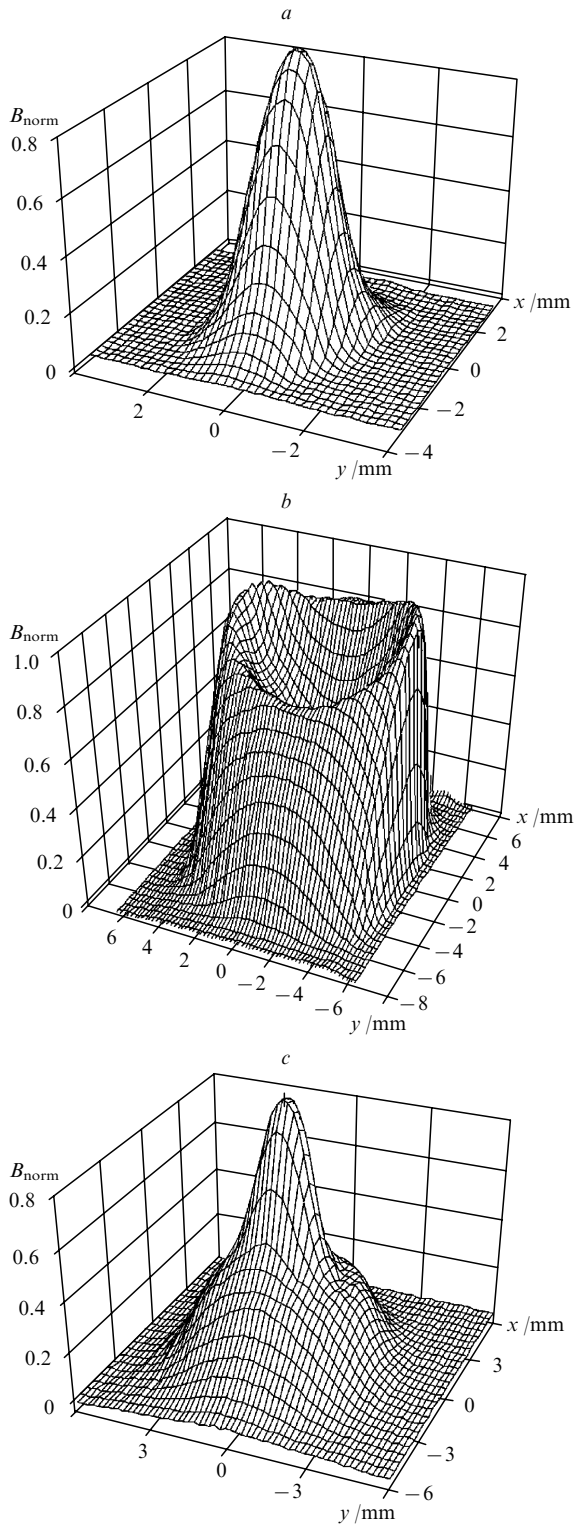


Figure 2. Spatial distributions of the normalised radiation intensity of a hollow cathode lamp (*a*), an electrodeless lamp (*b*) and a deuterium lamp (*c*) measured at the resonance wavelength of lead (283.3 nm).

† This techniques is called classical or conventional AAS.

fill-gas atoms. The distribution presented in Fig. 2 *a* is typical of most hollow cathode lamps. However, lamps designed for analysis of non-volatile elements include hollow cathodes with larger radii. In such hollow cathode lamps, electron impact excitation/ionisation can be accompanied by other processes. In particular, this is evidenced by the fact that the spatial intensity distribution for barium ion has a dip in the near-axis region due to Penning ionisation.[10]

2. Electrodeless discharge lamps

Hollow cathode lamps used in AAS for most analyte elements give rather intense and narrow spectral lines. However, electrodeless discharge lamps (EDL) offer better metrological characteristics for some volatile elements, such as As, Hg, Se, Cd, Pb, *etc*. The service time of these lamps is much longer and they give more intense (5–100-fold more intense) radiation at the resonance wavelengths than the corresponding hollow cathode lamps. Line spectra in EDL are excited by inductively coupled plasma generated in a sealed valve at a frequency of tens of megahertz (and higher). Argon or krypton is used as a fill gas at a pressure of $\sim$1 mm Hg. Analyte atoms are introduced into the high-frequency plasma by thermal vaporisation from the base of the valve as the latter is heated. Therefore, the valve must be preheated for 30–40 min to provide a steady-state mode.

The results of investigations of the spectral characteristics of EDL were summarised in a review.[13] The intensity distributions of electromagnetic fields were reported.[14–16] As in hollow cathode lamps, the widths of the spectral profiles are about 1 pm and are determined primarily by the hyperfine splitting and Doppler broadening. Spatial distributions of the radiation intensity in EDL for different elements with the use of different fill gases were examined.[17, 18] It was found that the excited argon atoms and ions are characterised by a dome-shaped distribution with the maximum radiation intensity in the near-axis region of plasma.[17] This distribution is due to direct (or stepwise) electron impact excitation.

The introduction of metal atoms substantially complicates the situation. In this case, the plasma in EDL becomes strongly structured. Clouds of metal and argon atoms are spatially separated. A typical radiation intensity distribution for metal atoms in the cross-section of EDL is exemplified by the radiation intensity distribution for lead at the resonance wavelength of 283.3 nm [17] presented in Fig. 2 *b*. It can be seen that this distribution is strongly non-uniform. A pronounced minimum is observed on the axis of the plasma and the radiation beam is located primarily in the narrow region along the walls of the valve (optical skin effect). Detailed studies demonstrated [17] that neither the electromagnetic skin effect nor self-absorption can account for such anomalous distributions. It was found [17] that the observed distributions are determined by the radial cataphoresis effect resulting in a strongly non-uniform distribution of neutral metal atoms with a maximum near the walls of the valve. Together with the dome-shaped distribution of the electron concentration, this leads to the spatial distribution of the excited atoms presented in Fig. 2 *b*.

3. Continuous spectrum radiation sources

In addition to line radiation sources, continuous spectrum radiation sources are also widely used in AAS. These are deuterium, hydrogen, xenon, tungsten and halogen lamps. Generally, xenon arc lamps are used as transmitted radiation sources for the detection of selective absorption,[19] whereas deuterium lamps are widely used for non-selective absorption correction.

In deuterium lamps, radiation is generated in a low-pressure non-self-sustained arc discharge. This discharge provides a high-intensity continuous spectrum in the 190–360 nm spectral range, which contains the majority of analytical lines used in AAS. Since electron impact is the main excitation channel in these sources,[20] the radiation intensity distribution is evidently determined by the electron concentration distribution in the positive column of an arc discharge. It was shown [20] that the maximum electron density occurs on the discharge axis and monotonically decreases toward its ends. Measurements of the spectral intensity distribution in the cross-section of a deuterium lamp confirmed the above suggestion. The spatial distribution of the spectral intensity of a deuterium lamp is presented in Fig. 2 *c*.[12] The distribution is dome-shaped with a maximum on the axis of the cathode hollow and minima at the cathode ends. A plateau present at the base of the distribution is associated with the presence of a circular screen near the arc cathode.

Analysis of the data presented in Fig. 2 showed that spatial distributions of radiation generated by sources used in AAS are strongly non-uniform (in the case of EDL, they are additionally non-monotonic), and the character of non-uniformity strongly depends on the type of the source.

4. Spatial structure of transmitted radiation in an atomiser

Special optics is used to convert the radiation from the source into a transmitted beam, which is directed to an atomiser. An optical system of an atomic absorption spectrometer focuses a source image onto the centre of the atomiser and then it is directed to the entrance slit of the monochromator with the use of another optical system. Then a probe beam, which is passed through an absorbing layer in the atomiser and through a narrow vertical slit of the monochromator is recorded by a detector at the outlet of the spectrometer. The spatial structure of the transmitted beam in an atomiser was examined.[21] A typical radiation intensity distribution in the transmitted beam produced by a lead hollow cathode lamp is shown in Fig. 3. Since a source image is formed in the

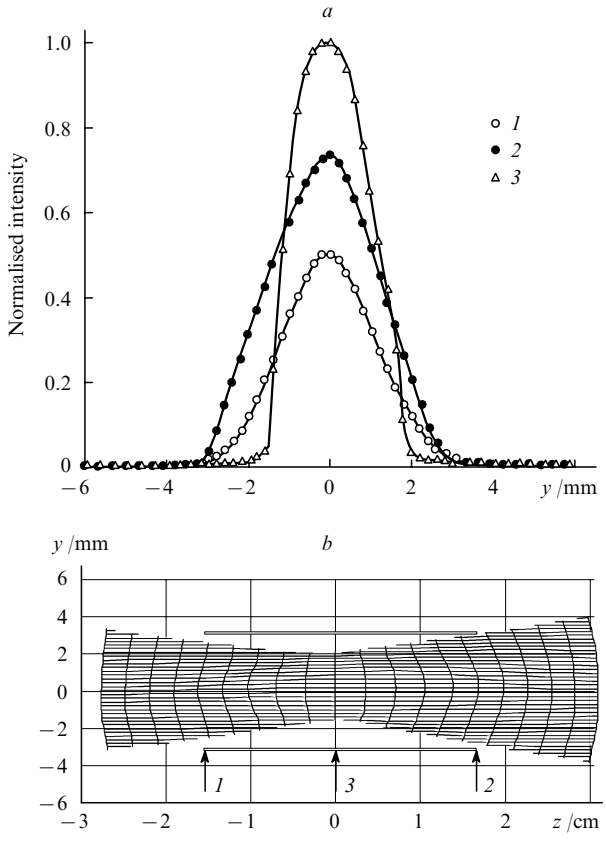


Figure 3. Radiation intensity distribution in the vertical cross-section of the transmitted beam at the inlet (*1*), at the output (*2*) and in the centre (*3*) of an atomiser (*a*) and the shape of the transmitted beam inside the atomiser (*b*);[21]
(*b*): horizontal lines indicate the walls of the tube atomiser and arrows show the cross-sections of the beam, in which curves *1–3* presented in (*a*) were measured.

centre of an atomiser, curve *3* coincides with the central cross-section of the distribution presented in Fig. 2 *a*. These results reveal an interesting fact. As can be seen from Fig. 3 *a*, the areas under the distribution curves differ from each other. The radiation intensity in the vertical cross-section at the inlet of the atomiser is much lower than that at the output. This accounts for the change in the shape of the cross-section of the beam as it passes through the atomiser. At the inlet and outlet of the atomiser, the beam is elongated in the horizontal and vertical directions, respectively.[21] Radial radiation intensity distributions analogous to those presented in Fig. 3 *a* were constructed with a step of 1 mm along the axis of beam propagation. As a result, the structure of the beam in the atomiser was quantitatively characterised. The beam thus constructed is shown in Fig. 3 *b*. It can be seen that the beam becomes narrower in the centre of the atomiser and again becomes broader at the outlet.

The spatial structure of the transmitted beam produced by electrodeless lamps is different in principle.[21] It should be noted that this beam is also characterised by a strongly non-uniform radiation intensity distribution.

III. Dynamics of spatial temperature distributions in atomisers

The overwhelming majority of substances analysed by atomic absorption methods exist in the condensed state. However, only free atoms in the gas phase can be detected by AAS. Consequently, it is necessary to convert the analyte into the gas phase before atomic absorption analysis. Atomisation is performed in atomisers with the use of different flames, plasma, laser radiation and electrothermal vaporisation (graphite atomisers). The main parameters governing the kinetics of vaporisation and atomisation, diffusion, absorption coefficients and distribution coefficients of atoms and molecules in an atomiser depend on the temperature.[22–24] Therefore, it is necessary to know the temperature field dynamics for the interpretation of all effects in AAS. Nowadays, only plasma and electrothermal atomisers are commercially produced, the latter being characterised by substantially more complicated temperature distributions and gradients. Below, we focus on the temperature fields in graphite electrothermal atomisers. The temperature fields in spectroscopic flames used for atomisation were examined.[25–28]

Graphite tube atomisers are used for converting an analyte from the condensed state into an atomic vapour by thermal vaporisation using fast (>2000 K s^{-1}) heating to $\sim$2000–3000 K. Presently, two types of electrothermal atomisers (with longitudinal and transverse heating) are commercially produced. In the former type of atomisers, a graphite tube is heated by passing the electric current along the tube [Heated Graphite Atomiser (HGA)]. In another type of atomisers, the electric current is passed transversely [Transversely Heated Graphite Atomiser (THGA)].

The temperature of the walls of tube atomisers is measured by optical pyrometry.[29–31] The temperature distributions on the surface of end-heated HGA-type atomisers are strongly non-uniform both in the longitudinal and radial directions. The dynamics of the longitudinal temperature distribution in a graphite tube during its heating to 2273 K is characterised by the plots presented in Fig. 4 *a*.[30] It can be seen that at the initial instant of time (within the first second), the temperature distribution along the atomiser is virtually uniform because thermal exchange is a sluggish process. Then the longitudinal temperature drops progressively increase as a result of heat transfer to cold contacts and, in a steady-state mode, the temperature drops are larger than 900 K.

The changes in the gas-phase temperature in electrothermal atomisers were studied by different methods.[31–33] Coherent anti-Stokes Raman scattering (CASR)[32, 34] proved to be the most informative for this purpose. This method allows one to record the gas temperature with a high space-time resolution. The gas-phase

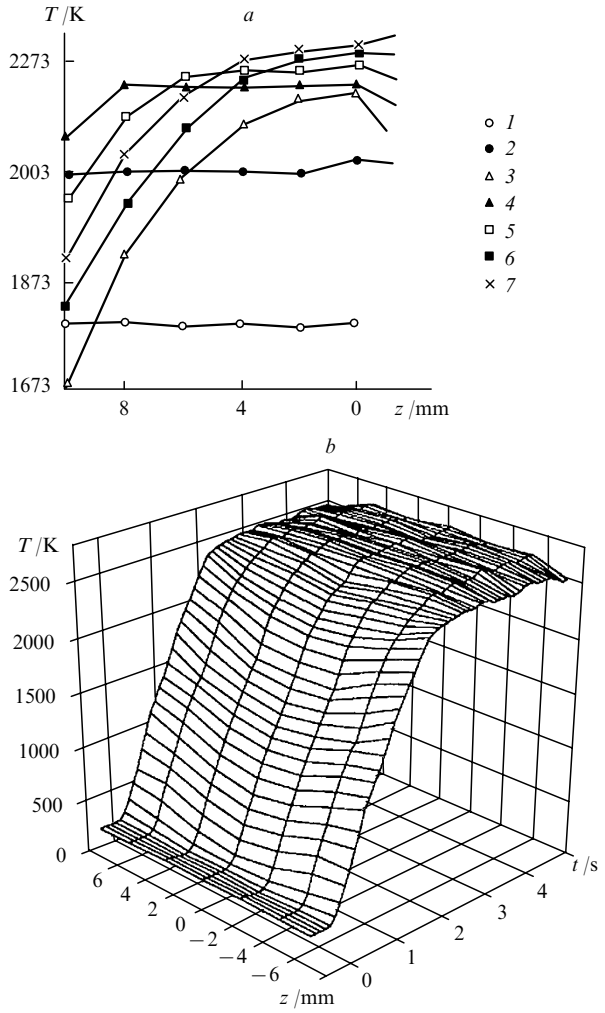


Figure 4. Plots characterising the space-time dynamics of the longitudinal temperature distributions in HGA- (*a*) and THGA-type (*b*) atomisers.
Time /s: (*1*) 0.8, (*2*) 1.0, (*3*) 10, (*4*) 1.2, (*5*) 1.5, (*6*) 3.0, (*7*) 2.0.

temperature depends substantially on protecting gas flows. In HGA-type atomisers, the gas-phase temperature drops in the longitudinal direction can be as large as 1500 K, and the drops in the radial direction can reach 800 K (with the use of a platform).[32, 35]

The temperature distributions in THGA-type atomisers were also studied by CASR. The changes in the gas-phase temperature along the axis of such atomisers are evident from the plots presented in Fig. 4 *b*.[34] It can be seen that THGA-type atomisers (unlike HGA-type atomisers) are virtually isothermal througout the tube length. As a result, the memory effects in measurements are reduced and the determination of non-volatile elements becomes much easier. However, the available THGA-type atomisers are not completely isothermal because substantial temperature gradients occur in the radial section, which is associated with the design parameters of these atomisers (see below).

IV. Three-dimensional structures of absorbing layers

1. Structure of absorbing layers in longitudinally heated atomisers

The dynamics of the formation and dissipation of absorbing layers in electrothermal atomisers was examined in numerous studies. The results of these investigations were summarised in monographs.[4, 31] However, only a few methods provide both the

time resolution and the spatial resolution in measurements. The spatial structures of absorbing layers are studied by Schlieren spectroscopy,[36] spatial separation[37] and different laser imaging techniques.[38–43] These methods were used in a series of studies aimed at atomising various elements. Shadow spectral filming[44] has gained wide acceptance. According to this method, monochromatic radiation at the wavelength of analyte atoms or molecules is passed through an atomiser. When this radiation is transmitted through the absorbing layer, a shadow image of a cloud of atoms (molecules or condensed nanoparticles) that absorb light at this wavelength appears on the detector surface. The higher the concentration of absorbing particles, the larger the absorbance of the shadow. The advantage of shadow spectral fiming is that it allows one to visualise the structures of layers consisting of different atoms (molecules or particles) that absorb in the 190–900 nm range with a space-time resolution in the cross-section of an atomiser.

a. Spatial distributions of free atoms

The dynamics of the formation and dissipation of absorbing layers of atoms of elements, which differ substantially in the physicochemical properties under different experimental conditions (atomisation from the walls and the platform in the gas-stop mode or purging with an inert gas), were studied by shadow spectral filming.[44–62] It was demonstrated that the structure of the absorbing layer is determined by physical (vaporisation, diffusion and convection mass transfer, condensation and revaporisation) and chemical (chemisorption, gas-phase and heterogeneous reactions) processes. The distributions of noble metal atoms in the cross-section of an atomiser appeared to be virtually uniform upon atomisation from both the platform and the walls of an atomiser.[40–42, 44–46, 63–65] A typical pattern giving an insight into the dynamics of the formation and dissipation of the absorbing layer of silver atoms is shown in Fig. 5 *a*. Each photograph in the figure is a monochromatic image of the inner surface of an atomiser with a platform. The measurements were carried out at the resonance wavelength of silver (328.1 nm). Silver atoms are vaporised from the platform, absorb light and are observed as a shadow image. The virtually uniform atom distribution in the cross-section of the atomiser is indicative of high efficiency of diffusion mass transfer (due to which the spatial non-uniformity of the distribution is smoothed) and the absence of chemical reactions involving silver atoms.

A completely different atomic distribution is observed in atomisers with internal inert gas purging. The absorbing layer

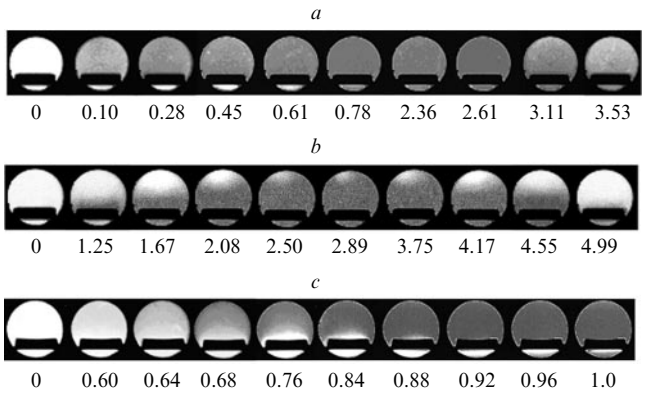


Figure 5. Images of the inner cavity of an HGA-type atomiser equipped with a platform, which were obtained by shadow spectral filming at the resonance wavelengths of silver (*a*, *b*) and gallium (*c*);[44, 47]
(*a*) 50 ng Ag, the gas stop mode; (*b*) 50 ng Ag, internal purging at a rate of 300 ml min^{-1}; (*c*) 50 ng Ga in the gas stop mode. Hereinafter, the time intervals from the onset of the atomisation cycle are given in seconds below the shots.

becomes strongly inhomogeneous with a sharp decrease in the atomic concentration from the bottom to the top of the atomiser (Fig. 5 *b*). This distribution is associated with the character of the inert gas flow. The gas enters from the ends of the atomiser and leaves the latter through a small dosing hole in the centre, which results in a substantial acceleration of the gas flow.

Anomalous effects were observed when performing atomisation of Group III elements (Al, In, Ga and Tl).[47–51] The dynamics of formation of an absorbing layer of gallium atoms is illustrated in Fig. 5 *c*. These results are indicative of a pronounced anomaly; that is, the atoms are introduced into the gas phase from the upper part of the atomiser rather than from the platform onto which a sample was dosed, *i.e.*, inverse atomisation occurs. This effect is attributed to initial vaporisation of a substance in the form of gallium suboxide molecules, which do not absorb at the atomic wavelength, and their reduction on the walls of the graphite atomiser followed by introduction of gallium into the gas phase, now, as free atoms.[44, 48]

The anisotropy of the propagation velocity of metal vapour in the longitudinal and cross-sections of the atomiser was revealed. Vapour diffusion along the atomiser tube occurs in a medium, in which the temperature sharply decreases (see Fig. 4 *a*), and the diffusion rate is limited by the velocity of thermal front propagation in this direction. In addition, some shots in Fig. 5 *c* show a sharp decrease in the concentration of atoms near the platform due to their condensation on the substantially colder platform. Then the condensed atoms again pass to the gas phase as the platform is heated. Therefore, the dynamics of formation and dissipation of an absorbing layer consisting of gallium atoms is complicated by the simultaneous occurrence of numerous physicochemical processes. Analogous features of the dynamics of formation of absorbing layers were revealed in studies of Tl, In, Ge and Bi atomisation.

An even more complicated dynamics was observed in studies of aluminium atomisation.[48, 52–54] The analytical signal recorded on a conventional Perkin-Elmer Zeeman 5000 atomic absorption spectrometer (Fig. 6 *a*) appears as a regular peak without anomalies. However, investigation of this process by shadow spectral filming revealed a series of effects, which were not manifested in the conventional absorption signal. Images obtained by digital shadow spectral filming (Fig. 6 *b*) show that the atomic distribution in the cross-section of the atomiser is strongly non-uniform. The maximum concentration is observed near the graphite walls, and the minimum is observed near the dosing hole. This is indicative of oxygen diffusion into the atomiser through the dosing hole and a high rate of gas-phase oxidation of aluminium. The near-axis region of the atomiser also contains a large amount of aluminium, but it is involved in oxides, which do not absorb at the atomic wavelength. A region selected by the entrance slit of the monochromator is indicated by a rectangle in shot 1 (see Fig. 6 *b*). The radiation from only this region is focused onto the detector and is recorded by a conventional atomic absorption spectrometer. In the plot $A(t)$ (see Fig. 6 *a*), the instant of time corresponding to this shot is indicated by point 1. The absorbance detected by a spectrometer at this instant of time is virtually equal to zero. However, the atomiser contains a substantial amount of aluminium atoms, which are located along the walls (see Fig. 6 *b*, shot 2) and are beyond the detection limit of conventional spectrometers.

The above results also suggest that free atoms are redistributed inside the atomiser. In the early steps of atomisation, the concentration of aluminium atoms is higher above the platform. In the final step, the concentration maximum is shifted to the region under the platform (see Fig. 6 *b*, shots 3 and 4). This additionally confirms a substantial role of oxygen in the distribution of aluminium. Evidently, the conditions under the platform are more reductive than those in the upper part of the atomiser. In addition to the above-mentioned anomalies of the atomic spatial distribution, atomisation of aluminium (as well as of ytterbium

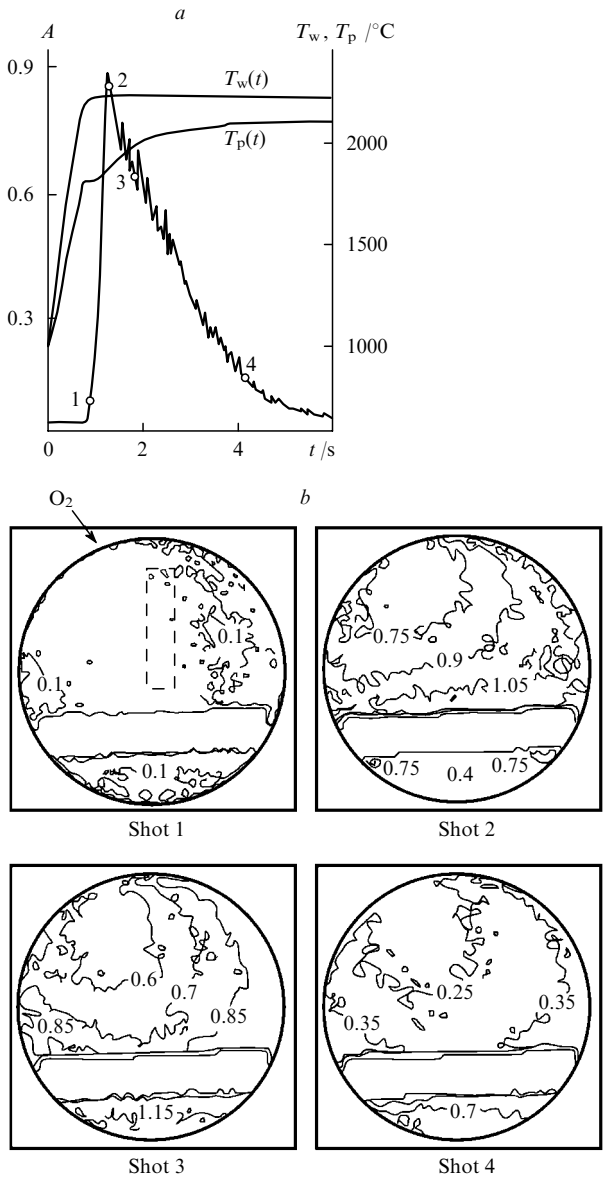


Figure 6. Results of the detection of platform atomisation of 15 ng of aluminium by atomic absorption (*a*) and spatially resolved digital shadow spectral filming (*b*);[53]
(*a*): points 1–4 in the plot $A(t)$ correspond to shots 1–4 in (*b*); $T_w(t)$ and $T_p(t)$ are the changes in the temperature of the walls and platform of the atomiser, respectively;
(*b*): contours of the absorbance are given, the arrow in shot 1 indicates the position of the dosing hole.

and some other elements) is accompanied by explosive atomisation.[53, 54, 66, 67]

The results obtained in the study [55] of boron atomisation also provide evidence that oxygen diffusion through the dosing hole has a strong effect on the atomic distribution of this element.

b. Spatial distributions of non-selectively absorbing particles

In electrothermal AAS, molecules play a very important role in the formation of free atoms.[68, 69] In addition, molecules are responsible for non-selective absorption.[70, 71] Studies of the dynamics of formation of molecular layers by shadow spectral filming also revealed a number of anomalies.[46, 48–51, 54, 56, 57] The structure evolution of an absorbing layer composed of gallium molecules in graphite tube atomisers is illustrated in Fig. 7 *a*. The images were obtained at the wavelength of 254 nm, where one of the molecular absorption maxima of gallium is located.

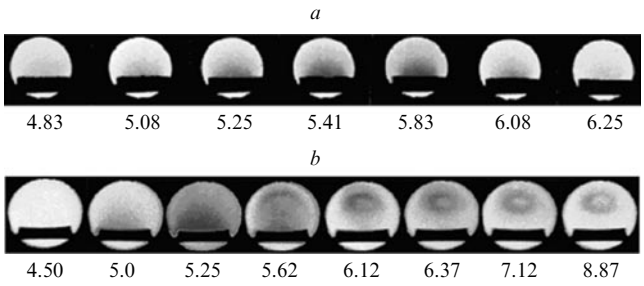


Figure 7. Images of the inner cavity of a graphite tube atomiser obtained by shadow spectral filming at a wavelength of 254 nm for vaporisation of 1 μg of Ga (*a*) and Al (*b*) salts.[48]

Contrary to the commonly accepted opinion that molecules are located at the colder ends of atomisers, their true distribution is quite opposite. Vaporisation leads to a strongly non-uniform distribution of molecules inside an atomiser. The concentration maximum is located near the platform, and the concentration minimum is near the graphite walls. No molecules are observed under the platform, whereas molecules are observable in the central regions of the atomiser. Taking into account this distribution, it was concluded that these are metal suboxide molecules. A comparison of the atomic (see Fig. 5 *c*) and molecular (see Fig. 7 *a*) distributions of gallium revealed the following fact. Molecules disappear in the regions where atoms appear. The same situation was observed in studies of the structures of absorbing layers composed of indium- and aluminium-containing molecules. This led to the conclusion that reduction of gaseous metal oxide on the graphite surface is a heterogeneous processes, which can be described in the general form by the equation

$$M_2O\,(g) + C\,(s) = 2\,M\,(g) + CO\,(g). \qquad (2)$$

This is one of the most important processes in electrothermal AAS.

Studies of absorbing layers of aluminium suboxide molecules showed yet another anomaly.[48, 54, 56] The dynamics of formation of such layers is typical of two-step processes. Initial vaporisation of molecules from the platform (the characteristic features of this process are virtually identical to those described above for gallium vaporisation) is followed by the formation of an absorbing cloud having a complicated toroidal structure inside the atomiser (Fig. 7 *b*). A detailed analysis demonstrated that the cloud consists of aluminium oxide nanoparticles condensed in the gas phase. Vaporisation of microgram amounts of various elements affords analogous structures consisting of nanoparticles. Therefore, not only atoms and molecules but also nanoparticles are present inside electrothermal atomisers at extremely high temperatures, and all these species are characterised by a strongly non-uniform spatial distribution.

2. Structures of absorbing layers in transversely heated atomisers

In the previous section, we noted that temperature fields in transversely heated atomisers differ radically from those in longitudinally heated atomisers.[58] Transversely heated graphite atomisers are almost longitudinally isothermal but are characterised by considerable temperature inhomogeneities in the cross-section.[59] This is responsible for the formation of new three-dimensional atomic, molecular and nanoparticulate structures in THGA.

a. Atomic distribution

The dynamics of formation and dissipation of an adsorbing layer of silver atoms in THGA [59] is evident from an analysis of the results of shadow spectral filming presented in Fig. 8 *a*. It can be seen that atoms appear directly above the bottom of the atomiser

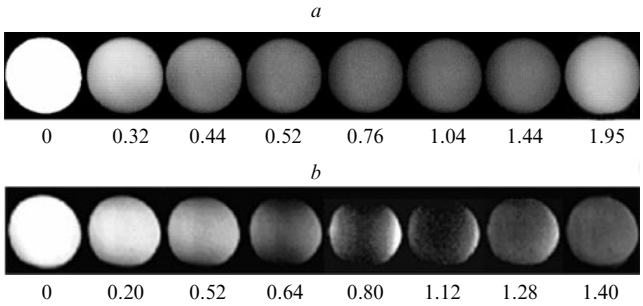


Figure 8. Images of the inner cavity of THGA obtained by shadow spectral filming for atomisation from the walls of 25 ng of Ag (*a*) and 200 ng of In (*b*).[59]

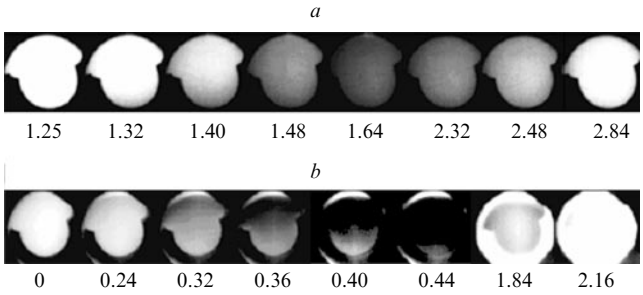


Figure 9. Images of the inner cavity of THGA with a platform obtained by shadow spectral filming for atomisation of 5 ng of Ag (*a*) and 675 ng of Ga (*b*).[59]

onto which a sample was dosed, and their spatial distribution in the initial step of atomisation is normal, *i.e.*, the atom concentration monotonically decreases from the bottom to the top. However, the absorbance maximum is gradually shifted to the side walls of the atomiser. This redistribution can be accounted for only by vapour adsorption (condensation) on colder regions followed by revaporisation during further heating of the atomiser. In the study,[47] a cascade mechanism of the substance transfer in the longitudinal direction of HGA-type atomisers was proposed. The same mechanism (but in the radial section) is observed in THGA-type atomiser. An analogous substance transfer in transversely heated atomisers was documented.[41,42] Interestingly, the vapour concentration is somewhat higher near the left side surface. This is due to the fact that the temperature in the left part of the tube in the atomiser used in experiments was somewhat lower than that in the right part because the cooling liquid is introduced from the left to the right contact.

The dynamics of formation and dissipation of an indium absorbing layer is presented in Fig. 8 *b*. A sample was dosed from the bottom of the tube.[59] It can be seen that the spatial atomic distribution is opposite to that observed in the case of silver atomisation. Indium atoms appear simultaneously in the upper and lower parts of the atomiser (shots obtained within 0.20 and 0.52 s after the onset of atomisation), and a pronounced absorbance minimum is observed on the side surfaces during the whole cycle. Analogous distributions are also typical of Ga, Tl and Bi atoms. It is known that, when vaporisation of aqueous samples of In, Tl, Bi and Ga is performed in graphite furnaces, oxides of these elements are the first to go into the vapour phase, and these oxides do not absorb at the resonance wavelengths of the corresponding atoms.[48] The effect presented in Fig. 8 *b* is indicative of decomposition of indium suboxide molecules. Evidently, the gas-phase temperature along the vertical diameter is higher than the decomposition temperature of oxides. This accounts for the minimum concentration of atoms near the side walls of the tube characterised by the lowest atomiser temperature.

Small inhomogeneities of the absorbing layer are observed during silver atomisation in THGA-type atomisers (Fig. 9 *a*). The atoms appear directly above the platform onto which a sample was dosed and gradually fill the whole volume of the atomiser (shots obtained within 1.32 and 1.40 s after the onset of the atomisation cycle). In this case, as in above-considered experiments (see Fig. 8 *a*), the vapour redistribution to the left side of the atomiser is observed (shots obtained within 2.32 and 2.84 s after the onset of the atomisation cycle). In the presence of a platform, this effect is less pronounced because atoms appear in the gas phase at a higher atomiser temperature. Analogous spatial structures of absorbing layers were observed also in manganese and copper atomisation. The observed atomic redistributions in the cross-section of atomisers also substantially influence the temperature gradients in atomisers.

The effect of inverse atomisation, which has been observed for the first time in HGA-type atomisers,[44,48] is clearly pronounced in the case of gallium atomisation in THGA-type atomisers equipped with a platform. The dynamics of the formation and dissipation of absorbing layers of gallium atoms is presented in Fig. 9 *b*.[60] An excess of gallium was used to improve visualisation of the process. As in the earlier study,[44] the characteristic features of the atomic distribution are attributed to the fact that gallium is initially vaporised as suboxides, which do not absorb at the atomic wavelength of 417.2 nm and, consequently, remain invisible in these measurements. Then suboxide molecules are reduced on the opposite surface of the atomiser (shots obtained within 0.24 – 0.40 s after the onset of the atomisation cycle) according to reaction (2).

An analogous dynamics of atomic spatial distributions was observed also for In, Tl and Bi atomisation. Therefore, inverse atomisation of Group III elements occurs also in THGA-types atomisers.

b. Molecules and condensed particles

The above-considered structures of absorbing layers were determined at wavelengths that did not overlap with the wavelengths of molecular absorption bands. Vaporisation of a salt containing 10 μg of indium was studied by shadow spectral filming and the results of this study are presented in Fig. 10 *a*. Shadow shots were measured at a wavelength of 294.4 nm [60] corresponding to the absorption maximum of indium suboxide.[48] It can be seen that a vapour cloud was initially formed at the bottom of the atomiser directly above the sample and had a normal three-dimensional structure (the vapour density monotonically decreases from the bottom to the top of the atomiser; see the shots obtained within 0.46 and 0.50 s after the onset of the atomisation cycle). However, the cloud is then transformed into a diffuse horizontal band between the side walls of the atomiser (shots obtained within 0.54 – 0.70 s after the onset of the atomisation cycle). In the final step of vaporisation, the band is broken and the vapour is accumulated near the side surfaces of the tube. The distributions

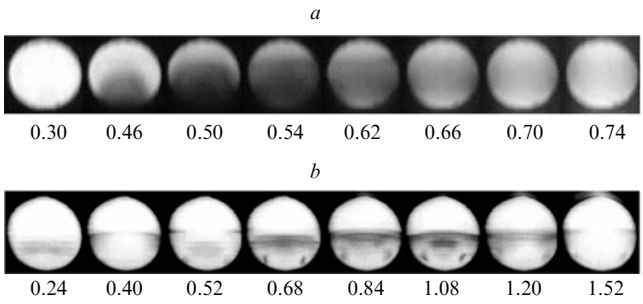


Figure 10. Images of the inner cavity of THGA obtained by shadow spectral filming for vaporisation from the wall of salts containing 10 μg of In (*a*) and 50 μg of $CaCl_2$ (*b*).[60,61]

of indium-containing molecules differ from those of indium atoms (see Fig. 8 *b*; the atoms were distributed along the vertical diameter of the atomiser, the density being higher at the ends). The observed three-dimensional structures of the absorbing layers are due to the characteristic features of the temperature gradients in the radial section of the atomiser.[59, 60] The lower-temperature region inside THGA-type atomisers is located along their horizontal diameter. Evidently, the lowest degree of dissociation of molecules occurs in this region. A higher-temperature region of the gas phase inside atomisers is located along the vertical diameter far from the cooled side contacts. It is this region where indium atoms are predominantly located.

Vaporisation of an excess of a substance in an atomiser gives rise to a cloud of condensed nanoparticles. Their distribution in the cloud is strongly non-uniform and complicated. The results of study of vaporisation of $CaCl_2$ (50 μg) in a THGA-type atomiser by shadow spectral filming are given as an example in Fig. 10 *b*. Visualisation was performed at a wavelength of 352 nm, which differs from the wavelengths of both molecular and atomic absorption bands. Therefore, it is evident that the above-considered structures of the absorbing layers are formed by particles condensed in the gas phase. Further studies demonstrated [60] that the absorbing cloud consists of nanoparticles the sizes of which are smaller than the wavelength of the light beam used. Interestingly, the absorbing cloud has a well-defined shape and is located along the horizontal diameter of the atomiser. This is consistent with the character of the temperature field distribution inside the atomiser. Evidently, vapour condensation should occur in lowest-temperature regions. However, shots obtained within 0.52 – 1.08 s after the onset of the atomisation cycle show an anomaly, *e.g.*, two small symmetrically arranged absorption regions appear in the lower part of the atomiser. This anomaly was reproduced in all experiments and its nature remains unclear. These regions can be due to the complex gas dynamics in atomisers as a result of the simultaneous occurrence of convective heat transfer from the ends of the tube and gas expansion caused by fast heating. The internal gas flow is also complicated by fast vaporisation of a considerable amount of the substance, which can cause a substantial change in the pressure distribution inside the atomiser. Under these conditions, the appearance of local vortex flows is probable, and the vapour can be partially trapped (and retained) by these flows. It should be noted that the cloud of condensed particles oscillates about the horizontal diameter of the atomiser (see Fig. 10 *b*), which is manifested as insignificant oscillations of absorption signals as the pulse is gradually changed.[62]

V. Influence of spatial inhomogeneities of absorbing layers on absorption

The above-considered data show that the distributions of all key parameters in AAS are characterised by spatial non-uniformity. This brings up the question of how these parameters influence the atomic absorption.

The spectrophotometric absorbance A serves as the analytical signal in AAS. In the ideal case of an infinitesimally narrow spectral line of the source and on the assumption that the absorbing layer is spatially homogeneous, the absorbance is proportional to the number of absorbing atoms [see Eqn (1)]. However, real measurements are performed with the use of sources the spectral lines of which are of finite width, for inhomogeneous absorbing layers. This substantially complicates the basic dependence of AAS, which has the following general form [72]

$$A = \log\left\{\left[\int_0^H\int_{-b/2}^{b/2}\int_{-\lambda^*}^{\lambda^*} J(x,y,-L/2)\,J(\lambda)\,\mathrm{d}x\mathrm{d}y\mathrm{d}\lambda\right]\times\right. \tag{3}$$

$$\times\left[\int_0^H\int_{-b/2}^{b/2}\int_{-\lambda^*}^{\lambda^*} J(x,y,-L/2)\,J(\lambda)\times\right.$$

$$\left.\left.\times\exp\left(-\int_{-L/2}^{L/2} K(x,y,z;\lambda)dz\right)\mathrm{d}x\mathrm{d}y\mathrm{d}\lambda\right]^{-1}\right\}.$$

In this equation, H and b are respectively the height and width of the transmitted radiation beam selected by the entrance slit of the monochromator, $\{-\lambda^*,\lambda^*\}$ is the spectral region selected by the monochromator (Fig. 11), $J(x,y,-L/2)$ is the intensity distribution of the transmitted beam at the entrance of the atomiser, L is the atomiser length, $J(\lambda)$ is a function describing the spectral profile of the incident beam, and $K(x,y,z,\lambda)$ is the absorption coefficient

$$K(x,y,z,\lambda) = C(\lambda,T)\,n(x,y,z),$$

where $C(\lambda,T)$ is the coefficient dependent on the temperature and spectral characteristics of the analytical line (the direct expression for this coefficient was reported in the study [24]) and $n(x,y,z)$ is the local concentration of absorbing particles.

From Eqn (3) it follows that the absorbance in conventional AAS depends on three factors: (1) spectral characteristics of the analytical line (the dependence of J, T and K on λ); (2) spatial distributions of absorbing particles and the atomiser temperature (the dependence of K on x, y and z); (3) spatial intensity distribution of the transmitted radiation beam. In the limiting case of the uniform distributions of absorbing particles, temperature and transmitted radiation intensity and on the assumption that the analytical line is single and infinitesimally narrow, the absorbance is directly proportional to the number of absorbing particles inside the atomiser at each instant of time. Equation (3) is substantially simplified and reduces to Eqn (1). The most comprehensive analysis of the influence of the spectral factors on the atomic absorption was performed in the study.[24] In the general case, the spectral profiles of emission lines $J(\lambda)$ and absorption lines $K(\lambda)$ are determined by Doppler and impact broadening, the absorp-

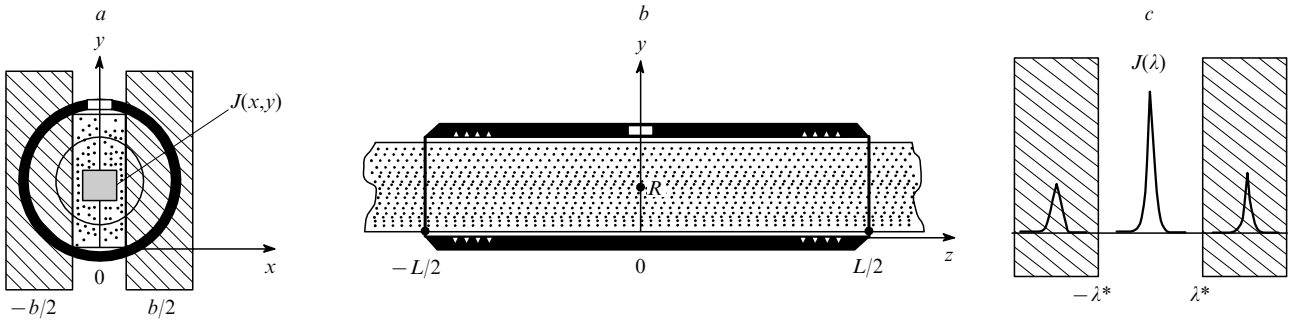


Figure 11. Cross- (*a*) and longitudinal sections (*b*) of a tube electrothermal atomiser and the transmitted beam as well as the spectral line $J(\lambda)$ selected within the transmitted band $\{-\lambda^*,\lambda^*\}$ of the monochromator (*c*).[24]

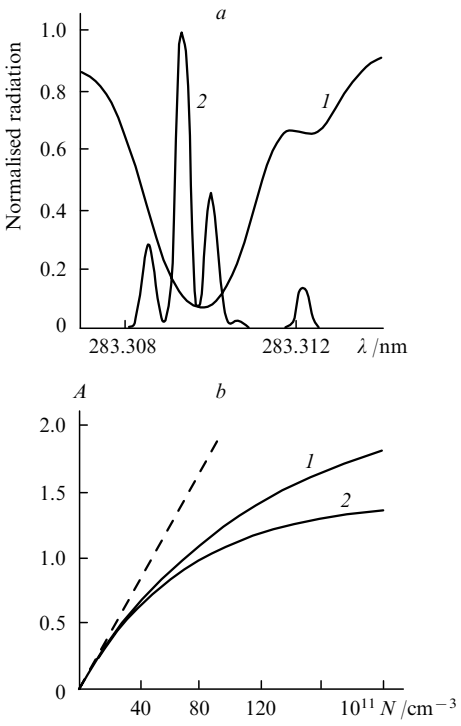


Figure 12. Spectral profiles of absorption (*1*) and emission (*2*) for the resonance line of Pb at 283.3 nm (*a*) and the dependence of the absorbance on the number of absorbing atoms for this line, which takes into account all spectral characteristics of the line (*1*) and inhomogeneity of the absorbing layer (*2*) (*b*).[24]

tion line shift and the hyperfine structure of the spectral transition. Figure 12 *a* gives the emission and absorption line contours for the resonance line of lead at 283.3 nm, which were calculated for the typical conditions of AAS taking into account the above-mentioned mechanisms of broadening.[24] The plot of the absorbance *vs*. the number of absorbing atoms corresponding to this spectral transition is shown in Fig. 12 *b* (curve *1*). In calculations of this dependence, the spatial distribution of absorbing atoms was assumed to be uniform. It can be seen that broadening of the spectral line leads to curving and a decrease in the slope of the plot $A = f(N)$, which are particularly substantial for the spectral lines consisting of far-separated hyperfine components.

In addition to the above-described spectral factors, the shapes of the concentration curves strongly depend on the spatial distributions of the temperature gradients in the atomiser and the concentration of absorbing atoms. This influence is manifested in two directions. The longitudinal temperature and concentration gradients lead to a decrease in the slope of the plot given by Eqn (3), whereas the transverse gradients lead to further curving (see Fig. 12 *b*, curve *2*).

The spectral transitions for some other elements were studied analogously. It was demonstrated [24] that the inhomogeneity of absorbing layers in the cross-section is one of the major factors responsible for curving of the calibration plots in AAS.

Therefore, the absorbance in conventional AAS depends not only on the number of absorbing atoms but also on their distribution inside the atomiser, as well as on the spatial structure of the probing beam, and is described by the following equation [72]

$$A = A_t(N) - \Delta A(N', J'),$$

in which the first term can be referred to as the true absorbance (which depends only on the number of absorbing atoms N) and the second term depends on the gradients of spatial distribution of atoms (N') and the transmitted radiation intensity (J') and is essentially the photometric error of the atomic absorption detection associated with inhomogeneity of the absorbing layer.

This error in conventional atomic absorption spectrometry is explained as follows. The luminous flux Φ_0 incident on the atomiser can be represented as consisting of n beams with intensity J_{i0} each. Then

$$\Phi_0 \sim \sum_{i=1}^{n} J_{i0}\,.$$

Analogously, the luminous flux Φ_t passed through the absorbing layer can be represented as

$$\Phi_t \sim \sum_{i=1}^{n} J_i\,,$$

where J_i is the local intensity of the probing beam passed through the corresponding region of the atomiser.

Therefore, the absorbance measured by conventional spatially integrated detection (SID) systems is described by the following equation:

$$A_{SID} = \log\frac{\Phi_0}{\Phi_t} = \log\frac{\sum J_{i0}}{\sum J_i}\,. \qquad (4)$$

As demonstrated above, the absorbance depends on all types of inhomogeneities and is not proportional to the number of absorbing atoms N. At the same time, the number of these atoms can be represented by the sum

$$N = \sum_{i=1}^{n} N_i \Delta S_i\,,$$

where N_i (in cm^{-2}) is the atom density in the ith beam and ΔS_i is the cross-section area of the ith beam. If the elemental beams have equal cross-sections,

$$\Delta S_i = \frac{S}{n}\,,$$

where S is the cross-section area of the total beam. Evidently, the local absorbance A_i becomes proportional to N_i as the transverse size of the beam decreases

$$A_i = \log\frac{J_{i0}}{J_i} \sim N_i\,.$$

Therefore, if the absorbance is represented as

$$A = \frac{1}{n}\sum_{i=1}^{n} A_i = \frac{1}{n}\sum_{i=,1}^{n} \log\frac{J_{i0}}{J_i}\,,$$

this parameter is proportional to the number of absorbing atoms regardless of their spatial distribution and the distribution of transmitted radiation intensity. Consequently, the spatially resolved detection (SRD) is required for correct photometric measurements of the absorbance of spatially inhomogeneous layers. The analytical signal A_{SRD} determined by the sum

$$A_{SRD} = \frac{1}{n}\sum_{i=1}^{n} \log\frac{J_{i0}}{J_i}\,, \qquad (5)$$

is the true absorbance, which depends on spatial inhomogeneities, *i.e*.,

$$A_{SRD} = A_t(N).$$

VI. Spatially resolved atomic absorption analysis

The above-formulated idea of the spatially resolved detection was realised in practice in the studies.[73, 74] Below we describe an original experimental apparatus for the space–time resolved light absorption detection. The new detection system includes a linear position-sensitive detector (a photodiode bar or a charge-

coupled device) vertically located along the exit slit of the monochromator in the plane optically coupled with the centre of the atomiser. In this method, in contrast to conventional AAS, the distribution of transmitted radiation intensity along the vertical diameter of the atomiser, rather than the spatially integrated luminous flux passed through the absorbing layer, is measured at each instant of time.

Let us consider an example of the detection for atomisation of 0.1 ng of cadmium from a platform. The spatial intensity distributions of the radiation beam from cadmium EDL passed through the atomiser under different conditions are shown in Fig. 13. The spectral intensity distribution at the resonance wavelength of 228.8 nm is qualitatively analogous to that presented in Fig. 2 *b*. The maximum is located at the periphery of the source. Since the diameter of EDL is approximately twice as large as the inner diameter of the atomiser (6 mm), the radiation beam from only one-half of the distribution shown in Fig. 2 *b* enters the system. The tube of the atomiser substantially shields the incident beam. Curve *1* in Fig. 13 shows the intensity distribution of the radiation beam, which is passed through the cylindrical tube of the atomiser, along the exit slit of the spectrometer.

In atomisers equipped with a platform, the lower part of this distribution is substantially transformed (curve *2*). The intensity near the platform ($y = 1$ mm) is equal to zero and has a small peak of the radiation beam passed under the platform ($y = 0.5$ mm). In conventional electrothermal AAS, a short slit (with a height of 2 mm) of the monochromator of the spectrometer is used to shield intrinsic emission of the atomiser. This slit selects a small region above the platform along the vertical diameter of the atomiser. This region is dashed in the inset to Fig. 13 and the spatial profile of EDL radiation passed through this short slit is shown by curve *3*. In conventional AAS, the total luminous flux passed through the short slit, *i.e.*, the surface area under curve *3*, rather than the intensity distribution is measured. In spatially resolved AAS, the profile of the radiation beam passed through the total cross-section of the tube, $J(y)$, (curve *2*) is measured at each instant of time. This is the main difference between the methods under consideration. Spatially resolved AAS is substantially more informative than conventional AAS.

The evolution of the distribution of transmitted radiation intensity $J(y,t)$ in the course of platform atomisation of 0.1 ng of cadmium is shown in Fig. 14. The intensity dip starting from 0.25 s is determined by resonance radiation absorption at a wavelength of 228.8 nm by cadmium atoms vapourised from the platform. After completion of the atomisation cycle ($t > 1.5$ s), the spatial profile of the incident beam is completely restored.

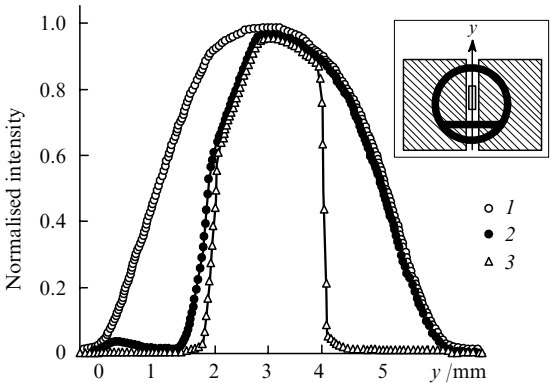


Figure 13. Intensity distribution of radiation from cadmium EDL passed through an atomiser without a platform (*1*), with a platform (*2*) and through a short monochromator slit (*3*).[79]
The cross-section of a tube atomiser equipped with a platform and regions inside the atomiser selected by tall and short slits is shown in the inset.

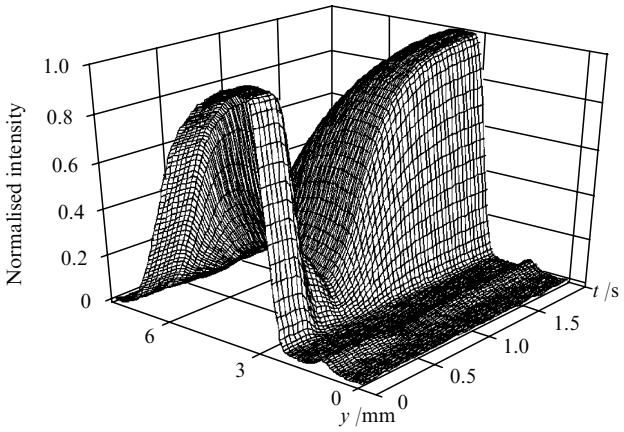


Figure 14. Changes with time in the spatial profile of the transmitted radiation intensity in the case of platform atomisation of 0.1 ng of Cd.[79]
The detection was carried out at the resonance wavelength of cadmium (228.8 nm).

With a knowledge of the changes with time in local intensities, it is easy to obtain spatially resolved absorbances $A_i(t)$ corresponding to the absorption in different regions of the atomiser along its vertical diameter. Therefore, the spatially resolved detection gives a family of pulses recorded in different regions of the absorbing layer (Fig. 15 *b*) instead of one atomic absorption

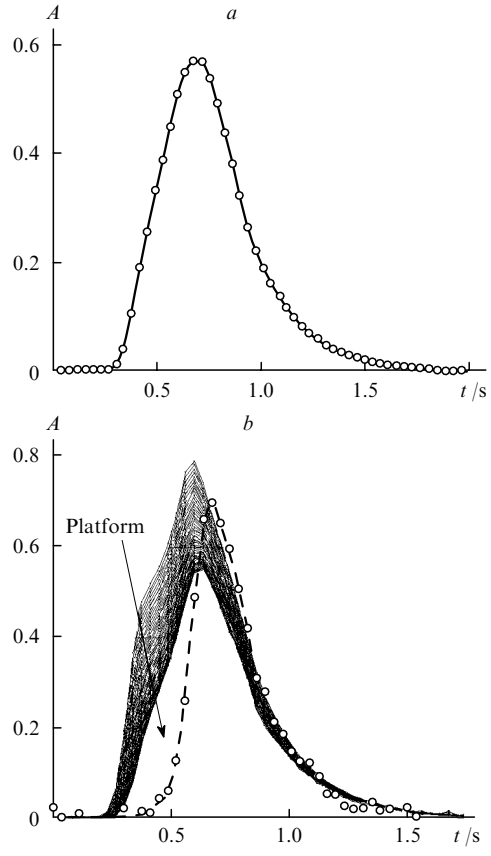


Figure 15. Absorption pulse obtained with the use of a conventional detection technique (*a*) and a family of 149 pulses obtained with the use of the spatially resolved detection (*b*) of atomisation in an HGA-type atomiser.[73]
The absorption pulse detected for a region under the platform is indicated by a dashed curve. The absorption pulses obtained when moving from the platform to the upper part of the atomiser are indicated by an arrow.

pulse integrated over the cross-section of the atomiser, which is obtained in conventional AAS (Fig. 15 *a*). Evidently, such a high spatial resolution is excessive. Consequently, the signals from the adjacent pixels of the detector can be combined to obtain the desired degree of spatial resolution. For HGA-type atomisers, depending on the degree of spatial inhomogeneity of particular distributions, 10–20 pulses along the diameter (6 mm) of an atomiser are sufficient.

The atomic absorption peaks monotonically decrease from the platform to the upper region of the atomiser (an arrow in Fig. 15 *b*). The integrated absorption

$$\int_0^\infty A_t(t)\mathrm{d}t,$$

which was measured directly above the platform onto which a sample was placed, is almost twice as large as the integrated absorption in the upper region of the atomiser. Interestingly, the radiation beam passes under the platform (see the small peak at $y = 0.5$ mm in Fig. 13), which makes it possible to obtain an atomic absorption pulse even from this region (the latter is indicated by a dashed curve in Fig. 15 *b*). It can be seen that cadmium atoms appear in the region under the platform with a substantial delay.

Atomic absorption spectrometry is widely used in fundamental physicochemical studies,[31] in particular, for the determination of the activation energies of vaporisation or atomisation. Evidently, the signal detected directly above the vaporisation source (the upmost curve in Fig. 15 *b*) most adequately describes the kinetics of sample vaporisation in the above-considered example. It can be seen that this signal is not an absorption monopulse, which is evidence that cadmium vaporisation occurs by a complex mechanism. In measurements with the use of conventional spatially integrated detection systems, these features become less pronounced (see Fig. 15 *a*), with the result that the activation energies of vaporisation are incorrect. In measurements with the use of spatially resolved detection systems, each measurement becomes much more informative due to which the conditions of atomisation and the formation of an absorbing layer of atoms can be better controlled.

A photometric error in the detection of atomic absorption of spatially inhomogeneous layers does not necessarily lead to an error in the determination of the number of absorbing atoms. If the character of spatial distribution of atoms in the analyte is identical to that in a reference sample, conventional atomic absorption analysis provides correct results. However, the spatial distribution of an analyte often depends substantially on the influence of the matrix of the analyte. In this case, the photometric error necessarily leads to an analytical error. This is clearly demonstrated by the following example.[74] Figure 16 *a* shows the dynamics of changes in non-selective absorption detected at the resonance wavelength of cadmium (228.8 nm) for atomisation of the certified reference sample SRM 1572 (Citrus Leaves). The distributions are clearly non-uniform, the absorbance being changed by a factor of 10–20 from the platform ($y = 0$) to the upper wall of the atomiser ($y = 3$ mm). The pulses of space-time resolved selective absorption of cadmium atoms shown in Fig. 16 *b* are characterised by substantially larger spatial gradients than those observed for atomisation from aqueous solutions (see Fig. 15 *b*). In this case, the difference (relative change) between the analytical signals

$$\int_0^\infty A_{\mathrm{SID}}(t)\mathrm{d}t \text{ and } \int_0^\infty A_{\mathrm{SRD}}(t)\mathrm{d}t$$

is 86%. In atomic absorption spectrometry with the use of the conventional (spatially integrated) detection, this leads to an analytical error of 67%. The possibility of appearing a considerable analytical error associated with the photometric error

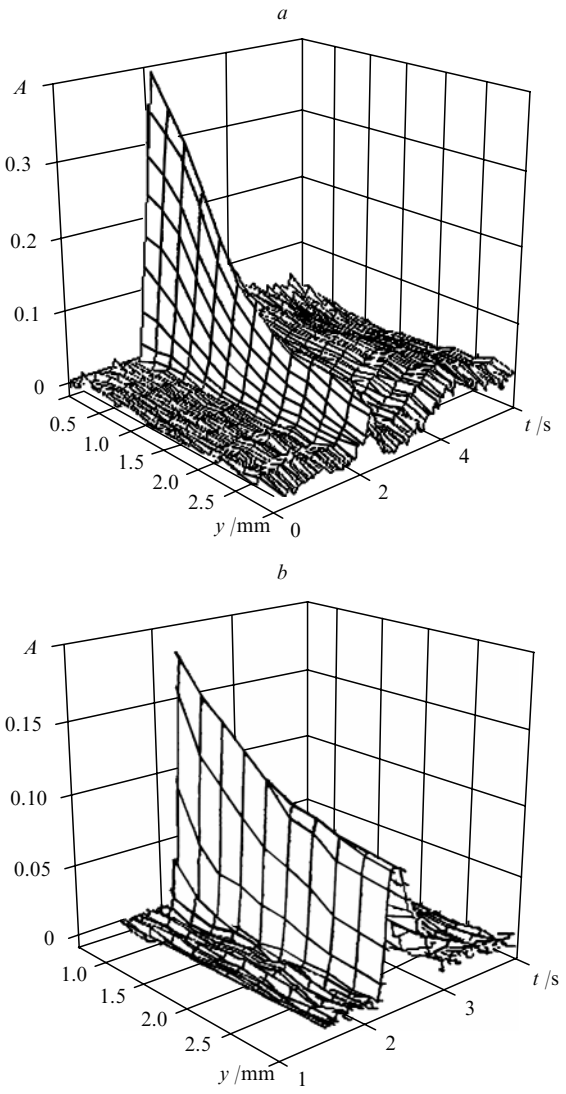


Figure 16. Space–time distribution of non-selective (*a*) and selective (*b*) absorption measured at the resonance wavelength of cadmium (228.8 nm) in the detection of cadmium in a certified sample SRM 1572 (Citrus Leaves).[74]

in measurements with the use of the conventional detection of inhomogeneous layers was also demonstrated.[75]

It is necessary to use matrix modifiers in electrothermal atomic absorption analysis of most substances. Taking into account the above-considered data, it is evident that the matrix modification of a sample leads not only to the known effect of separation of vaporisation of the analyte and the matrix but also to a unified spatial distribution of the analyte when it is atomised from an aqueous reference sample and from a real sample.

In conventional atomic absorption spectrometers, short monochromator slits are used with the aim of shielding intrinsic emission of the atomiser (see the rectangular region in the first shot in Fig. 6 *b* and the inset to Fig. 13). Tall slits used in spatially resolved spectrometers provide the space-time resolved detection of radiation beams from both a source and the walls and platform of the atomiser. The results of these studies can be used for the on-line monitoring of temperature changes. An example is illustrated in Fig. 17. Thermal emission from the platform and walls sharply increases as their temperature raises and the detection wavelength increases. In this example, the measurements were performed at the resonance wavelength of calcium (422.7 nm) in the visible spectral region. The peaks corresponding to glow of the

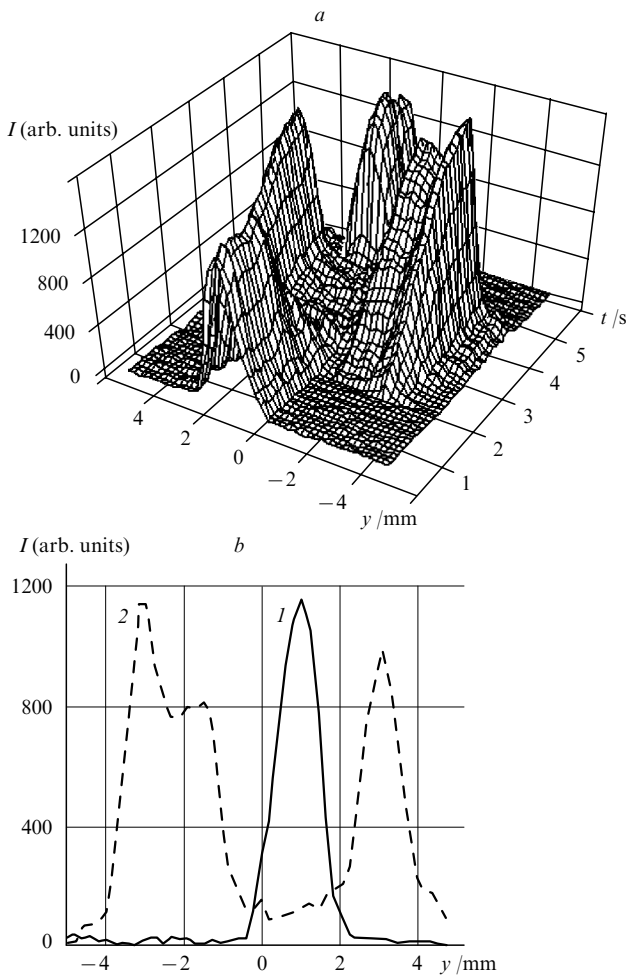


Figure 17. Changes in the intensity (I) of the radiation from the source, the walls and the platform of a tube atomiser measured with the use of the space-time resolved detection for calcium atomisation (*a*) and the radiation intensity distribution along the vertical diameter of the atomiser before atomisation (*1*) and at the instant when the maximum absorption was achieved (*2*) (*b*).[73]
Calcium atomisation from the platform, λ = 422.7 nm, T = 2500 °C.

walls of the atomiser and the platform are seen in Fig. 17 *a*. Before heating of the atomiser, when its walls are cold, only the intensity profile of the source is detected (curve *1*, Fig. 17 *b*). At the instant the atomisation temperature is achieved, the intensity profile of the transmitting source virtually disappears (vaporisation of a large amount of absorbing calcium atoms occurs), but three other peaks corresponding to emission from the upper and lower walls and the platform of the atomiser appear (curve *2*, Fig. 17 *b*). Changes with time in emission from the walls of the atomiser and the platform follow directly after a rise of the atomiser temperature (see Fig. 17 *a*). This fact can be used to estimate quantitatively the degree of heating of the system. The relative peak intensities of emission from the upper and lower walls strongly depend on the alignment of the atomiser.[76] The difference in the peaks of emission from the walls (see curve *2*, Fig. 17 *b*) indicates that the measurements were performed so that the atomiser tube was inclined to the optical axis of the spectrometer. This information can be used for the quantitative control of the alignment of the atomiser. The spatially resolved detection provides the possibility of seeing the exact position of the transmitted beam relative to the axis of the atomiser (see curve *1* in Fig. 17 *b*), which also substantially simplifies the alignment of the radiation source.

With a knowledge of the transmitted radiation intensities measured with the use of space-time resolved detection systems (see Fig. 14), it is always possible to obtain the absorption signal, which can be detected by a conventional spectrometer. For this purpose, it is sufficient to process the measured data according to Eqn (4). Therefore, AAS with the spatially resolved detection has all advantages of conventional AAS and includes them as a special case.

An idea of absolute atomic absorption analysis has been proposed back in 1955,[2] which marked the beginning of the development of analytical AAS. Over the history of AAS, this idea was extensively developed.[77–79] Taking into account the above-considered results of investigation of spatial distributions and their influence on the formation of analytical signals, it is evident that reference-free atomic absorption analysis cannot be performed without the space–time resolved detection.[80, 81]

Consequently, AAS with the spatially resolved detection appeared as the development of conventional AAS. The inclusion of additional measurements, *i.e.*, the measurements of the dependence of the key parameters on the spatial coordinate, provides substantially more informative data and higher accuracy of atomic absorption analysis.

VII. Conclusion

The development of methods and apparatuses, which could give higher-quality analytical signals, is one of the main fields of instrumental analytical chemistry. Atomic absorption signals detected in conventional AAS depend not only on the atomic concentration of the analyte element (the informative component of the signal), but also on their spatial distribution and the distribution of transmitted radiation intensity (the interference component of the signal). In AAS with the use of the spatially resolved detection, atomic absorption signals are independent of the spatial effects, due to which the resulting analytical signals are of higher quality. The present review shows that the key parameters of AAS (the atomiser temperature, distributions of atoms, molecules and condensed particles and transmitted radiation intensities) are characterised by a high degree of spatial inhomogeneities. The atomic absorption signal depends on these inhomogeneities, which are responsible for the photometric error in measurements with the use of conventional AAS. The absorption in spatially inhomogeneous media can be correctly measured only with the use of the spatially resolved detection. The above-considered examples of atomic absorption analysis of real substances confirm the practical importance of spatially resolved AAS.

According to the general classification of analytical chemistry methods,[82] AAS with the spatially resolved detection is a second-order method, because it provides two-dimensional data sets, *viz.*, the absorbance as a function of the time and the spatial coordinate. Conventional AAS belongs to first-order methods. A higher order of a method always provides higher-quality analytical signals.[82]

This review has been written with the financial support of the Russian Foundation for Basic Research (Project No. 05-03-04001NNIO_a).

References

1. B V L'vov *Zh. Anal. Khim.* **60** 434 (2005) [a]
2. A Walsh *Spectrochim. Acta* **7** 108 (1955)
3. B V L'vov *Atomno-absorbtsionnyi Spektral'nyi Analiz* (Atomic Absorption Spectral Analysis) (Moscow: Nauka, 1966)
4. B Welz, M Sperling *Atomic Absorption Spectrometry* (Weinheim: VCH, 1997)
5. H Falk *Prog. Anal. Spectrosc.* **5** 205 (1982)
6. S Caroli *Improved Hollow Cathode Lamps for Atomic Spectroscopy* (New York: Wiley, 1985)
7. J V Sullivan *Prog. Anal. At. Spectrosc.* **4** 311 (1981)

8. S Caroli *J. Anal. At. Spectrom.* **2** 661 (1987)
9. P L Larkins *J. Anal. At. Spectrom.* **7** 265 (1992)
10. A Kh Gilmutdinov, B Radziuk, M Sperling, B Welz, K Yu Nagulin *Appl. Spectrosc.* **49** 413 (1995)
11. A Kh Gilmutdinov, K Yu Nagulin *Zh. Prikl. Spektrosk.* **63** 895 (1996) [b]
12. K Yu Nagulin, A Kh Gilmutdinov *Zh. Prikl. Spektrosk.* **67** 143 (2000) [b]
13. J Sneddon, R F Browner, P N Keliher, J D Winefordner, D J Butcher, R G Michel *Prog. Anal. Spectrosc.* **12** 369 (1989)
14. J W Denneman *J. Phys. D: Appl. Phys.* **23** 193 (1990)
15. G G Lister, M Cox *Plasma Sources Sci. Technol.* **1** 67 (1992)
16. R B Piejak, V A Godyak, B M Alexandrovich *Plasma Sources Sci. Technol.* **1** 179 (1992)
17. A Kh Gilmutdinov, B Radziuk, M Sperling, B Welz, K Yu Nagulin *Appl. Spectrosc.* **50** 483 (1996)
18. K Yu Nagulin, A Kh Gilmutdinov, O R Badrutdinov *Zh. Prikl. Spektrosk.* **67** 15 (2000) [b]
19. B Welz, H Becker-Ross, S Florek, U Xeitmann *High-Resolution Continuum Source AAS* (New York: Wiley, 2005)
20. A Hoffmann, E Smolka, H Popp *Appl. Opt.* **31** 3540 (1992)
21. A Kh Gilmutdinov, B Radziuk, M Sperling, B Welz, K Yu Nagulin *Spectrochim. Acta, Part B* **51** 931 (1996)
22. W Frech, D C Baxter, E Lundberg *J. Anal. At. Spectrom.* **3** 21 (1988)
23. W Frech, M Arshadi, D C Baxter, B Hütsch *J. Anal. At. Spectrom.* **4** 625 (1989)
24. A Kh Gilmutdinov, T M Abdullina, S F Gorbachev, V L Makarov *Spectrochim. Acta, Part B* **47** 1075 (1992)
25. J Wang, S Li, X Wang, W Li, Z Chen, Y Luo *Spectrosc. Lett.* **25** 769 (1992)
26. J B Willis *Spectrochim. Acta, Part B* **52** 667 (1997)
27. R Azzoni, S Ratti, S K Aggarwal *Combust. Flame* **119** 23 (1999)
28. V V Toro, A J Mokhov, H B Levinsky, M D Smooke *Proc. Combust. Inst.* **30** 485 (2005)
29. H Falk *Spectrochim. Acta, Part B* **39** 387 (1984)
30. H Falk, A Glismann, L Bergann, G Minkwitz, M Schubert, J Skole *Spectrochim. Acta, Part B* **40** 533 (1985)
31. K W Jackson (Ed.) *Electrothermal Atomization for Analytical Atomic Spectrometry* (New York: Wiley, 1999)
32. B Welz, M Sperling, G Shlemmer, N Wenzel, G Marowsky *Spectrochim. Acta, Part B* **43** 1187 (1988)
33. S Wu, C L Chakrabarti, J T Rogers *Prog. Anal. Spectrosc.* **10** 111 (1987)
34. M Sperling, B Welz, J Hertzberg, C Rieck, G Marowsky *Spectrochim. Acta, Part B* **51** 897 (1996)
35. G Schlemmer, B Radziuk *Analytical Graphite Furnace Atomic Absorption Spectrometry* (Basel: Birkhauser Verlag, 1999)
36. D J Stafford, J A Holcombe *J. Anal. At. Spectrom.* **3** 35 (1988)
37. J A Holcombe, T E Histen *Spectrochim. Acta, Part B* **51** 1045 (1996)
38. C W Huie, C J Curran *Appl. Spectrosc.* **42** 1307 (1988)
39. C W Huie, C J Curran *Appl. Spectrosc.* **44** 1329 (1990)
40. E Masera, P Mauchien, Y Lerat *J. Anal. At. Spectrom.* **10** 137 (1995)
41. E Masera, P Mauchien, Y Lerat *Spectrochim. Acta, Part B* **54** 1007 (1996)
42. E Masera, P Mauchien, B Remy *J. Anal. At. Spectrom.* **11** 213 (1996)
43. N Hadgu, J Gustafsson, W Frech, O Axner *Spectrochim. Acta, Part B* **53** 923 (1998)
44. A Gilmutdinov, Yu Zakharov, V Ivanov, A Voloshin *J. Anal. At. Spectrom.* **6** 505 (1991)
45. A Kh Gilmutdinov, Yu A Zakharov, V P Ivanov, A V Voloshin *Zh. Anal. Khim.* **48** 28 (1993) [a]
46. N A Panichev, Q Ma, R E Sturgeon, C L Chakrabarti, V Pavski *Spectrochim. Acta, Part B* **54** 719 (1999)
47. A Gilmutdinov, Yu Zakharov, V Ivanov, A Voloshin *J. Anal. At. Spectrom.* **8** 387 (1993)
48. A Gilmutdinov, Yu Zakharov, V Ivanov, A Voloshin, K Dittrich *J. Anal. At. Spectrom.* **7** 675 (1992)
49. A Kh Gilmutdinov, Yu A Zakharov, V P Ivanov, A V Voloshin *Zh. Anal. Khim.* **49** 150 (1994) [a]
50. A Kh Gilmutdinov, Yu A Zakharov, V P Ivanov, A V Voloshin *Zh. Anal. Khim.* **49** 157 (1994) [a]
51. W Frech, D C Baxter *Spectrochim. Acta, Part B* **51** 961 (1996)
52. A Kh Gilmutdinov, Yu A Zakharov, V P Ivanov, A V Voloshin *Zh. Prikl. Spektrosk.* **53** 359 (1990) [b]
53. A Chakrabarti, A Gilmutdinov, C Hutton *Anal. Chem.* **65** 716 (1993)
54. A Kh Gilmutdinov, Yu A Zakharov, V P Ivanov, A V Voloshin, K Dittrich *Zh. Anal. Khim.* **49** 361 (1994) [a]
55. D M Goltz, C L Chakrabarti, R E Sturgeon, D M Hughes, D C Gregoire *Appl. Spectrosc.* **49** 1006 (1995)
56. A Kh Gilmutdinov, Yu A Zakharov, V P Ivanov, A V Voloshin *Zh. Anal. Khim.* **48** 812 (1993) [a]
57. A Kh Gilmutdinov, Yu A Zakharov, V P Ivanov, A V Voloshin *Zh. Anal. Khim.* **48** 1906 (1993) [a]
58. M Sperling, B Welz, J Hertzberg, C Rieck, G Marowsky *Spectrochim. Acta, Part B* **51** 897 (1997)
59. A Kh Gilmutdinov, A V Voloshin, Yu A Zakharov *Spectrochim. Acta, Part B* **60** 511 (2005)
60. A Kh Gilmutdinov, A V Voloshin, Yu A Zakharov *Spectrochim. Acta, Part B* **60** 1423 (2005)
61. A V Voloshin, A Kh Gilmutdinov, Yu A Zakharov *Zh. Anal. Khim.* **59** 154 (2004) [a]
62. A V Voloshin, A Kh Gilmutdinov, Yu A Zakharov, A A Sevast'yanov *Zh. Anal. Khim.* **59** 267 (2004) [a]
63. R W Fonseca, J McNally, J A Holcombe *Spectrochim. Acta, Part B* **48** 79 (1993)
64. O A Güell, J A Holcombe *J. Anal. At. Spectrom.* **7** 135 (1992)
65. J G Jackson, R W Fonseca, J A Holcombe *J. Anal. At. Spectrom.* **9** 167 (1994)
66. M M Lamoureux, C L Chakrabarti, J C Hutton, A Kh Gilmutdinov, Yu A Zakharov, D C Gregoire *Spectrochim. Acta, Part B* **50** 1847 (1995)
67. B V L'vov, A O Dyakov, A A Vasilevich, J W H Lam, R E Sturgeon *J. Anal. At. Spectrom.* **15** 115 (2000)
68. J A Holcombe, D L Styris, J D Harris *Spectrochim. Acta, Part B* **46** 629 (1991)
69. A De Vyt, R Gijbers, H Davock, C Van Roost, I Geuens *J. Anal. At. Spectrom.* **14** 499 (1999)
70. W Frech, B V L'vov, N P Romanova *Spectrochim. Acta, Part B* **47** 1461 (1992)
71. B V L'vov *Zh. Anal. Khim.* **30** 1870 (1975) [a]
72. A Kh Gilmutdinov, K Yu Nagulin, Yu A Zakharov *J. Anal. At. Spectrom.* **9** 643 (1994)
73. A Kh Gilmutdinov, B Radziuk, M Sperling, B Welz *Spectrochim. Acta, Part B* **51** 1023 (1996)
74. A Kh Gilmutdinov, K Yu Nagulin, M Sperling *J. Anal. At. Spectrom.* **15** 1375 (2000)
75. J Harnly, A Gilmutdinov, M Schuetz, J Murphy *J. Anal. At. Spectrom.* **16** 1241 (2001)
76. A R Somov, A Kh Gilmutdinov *Spectrochim. Acta, Part B* **52** 1413 (1997)
77. B V L'vov *Spectrochim. Acta, Part B* **33** 153 (1978)
78. B V L'vov *Spectrochim. Acta, Part B* **45** 633 (1990)
79. B V L'vov *J. Anal. Chem.* **355** 222 (1996)
80. A Kh Gilmutdinov, J M Harnly *Spectrochim. Acta, Part B* **53** 1003 (1998)
81. B V L'vov *Spectrochim. Acta, Part B* **54** 1637 (1999)
82. K S Booksh, B R Kowalski *Anal. Chem.* **66** 782A (1994)

[a] — *J. Anal. Chem. (Engl. Transl.)*
[b] — *J. Appl. Spectrosc. (Engl. Transl.)*